

# Statistical features of eddies approaching the Kuroshio east of Taiwan Island and Luzon Island

Yu-Hsin Cheng<sup>1</sup> · Chung-Ru Ho<sup>2</sup> · Quanan Zheng<sup>3</sup> · Bo Qiu<sup>4</sup> · Jianyu Hu<sup>1</sup> · Nan-Jung Kuo<sup>2</sup>

Received: 9 August 2016 / Revised: 5 January 2017 / Accepted: 5 January 2017 / Published online: 19 January 2017  
© The Oceanographic Society of Japan and Springer Japan 2017

**Abstract** This study examined the statistical features of eddies approaching the Kuroshio east of Taiwan Island and Luzon Island. In total, 315 eddies (138 anticyclonic and 177 cyclonic eddies) were detected from 19.5 years of satellite altimeter sea-level data, with more than 95% of these eddies being generated in the ocean west of the Mariana Islands. Eddy trajectory statistics indicated that eddies frequently intrude into the Kuroshio regime at two latitude bands, namely 18°N–19°N and 22°N–23°N, with periods of  $146 \pm 62$  and  $165 \pm 46$  days, respectively. The interaction time is longer within the two active bands ( $33 \pm 10$  days at

18°N–19°N and  $45 \pm 17$  days at 22°N–23°N) than at other latitudes. These two eddy-intrusion bands are associated with the northern and southern Subtropical Countercurrents (STCCs). These STCCs have a vertically reversed sign of the meridional potential vorticity gradient, thus providing a key energy source for eddy generation. In addition, when westward-propagating eddies approach the Ryukyu Islands, the southwestward recirculation flow east of the island chain as well as topographic effects cause some eddies to head southwestward to the east of Taiwan and intrude into the Kuroshio at 22°N–23°N, rather than to dissipate directly. Therefore, we suggest that the STCCs play a key role in inducing the eddies to frequently intrude into the Kuroshio at 18°N–19°N and 22°N–23°N. In addition, the Ryukyu Islands are responsible for concentrating the eddies within 22°N–23°N.

✉ Yu-Hsin Cheng  
yuhsin@xmu.edu.cn

Chung-Ru Ho  
b0211@mail.ntou.edu.tw

Quanan Zheng  
qzheng2@umd.edu

Bo Qiu  
bo@soest.hawaii.edu

Jianyu Hu  
huji@xmu.edu.cn

Nan-Jung Kuo  
C0021@mail.ntou.edu.tw

**Keywords** Ocean eddy · Kuroshio · Subtropical Countercurrent · Ryukyu Islands · Satellite altimetry

## 1 Introduction

The westward-flowing North Equatorial Current bifurcates into the northward Kuroshio and the southward Mindanao Current upon approaching the coast of the Philippines between 12°N and 15°N (Qiu 2001). The Kuroshio, which originates east of Luzon Island, is a western boundary current in the North Pacific (Fig. 1). Kida et al. (2015) reviewed oceanic fronts and jets in the western North Pacific, and showed that the Subtropical Countercurrents (STCCs) consist of multiple eastward-flowing bands. An earlier study (Hasunuma and Yoshida 1978) of a climatological dynamic height map revealed three separate eastward flows along 19°N–20°N (southern STCC),

<sup>1</sup> State Key Laboratory of Marine Environmental Science, College of Ocean and Earth Sciences, Xiamen University, Xiping Bldg, Xiang'an Campus, Xiamen 361102, Fujian, China

<sup>2</sup> Department of Marine Environmental Informatics, National Taiwan Ocean University, Keelung, Taiwan

<sup>3</sup> Department of Atmospheric and Oceanic Science, University of Maryland, College Park, College Park, MD, USA

<sup>4</sup> Department of Oceanography, University of Hawaii at Manoa, Honolulu, HI, USA

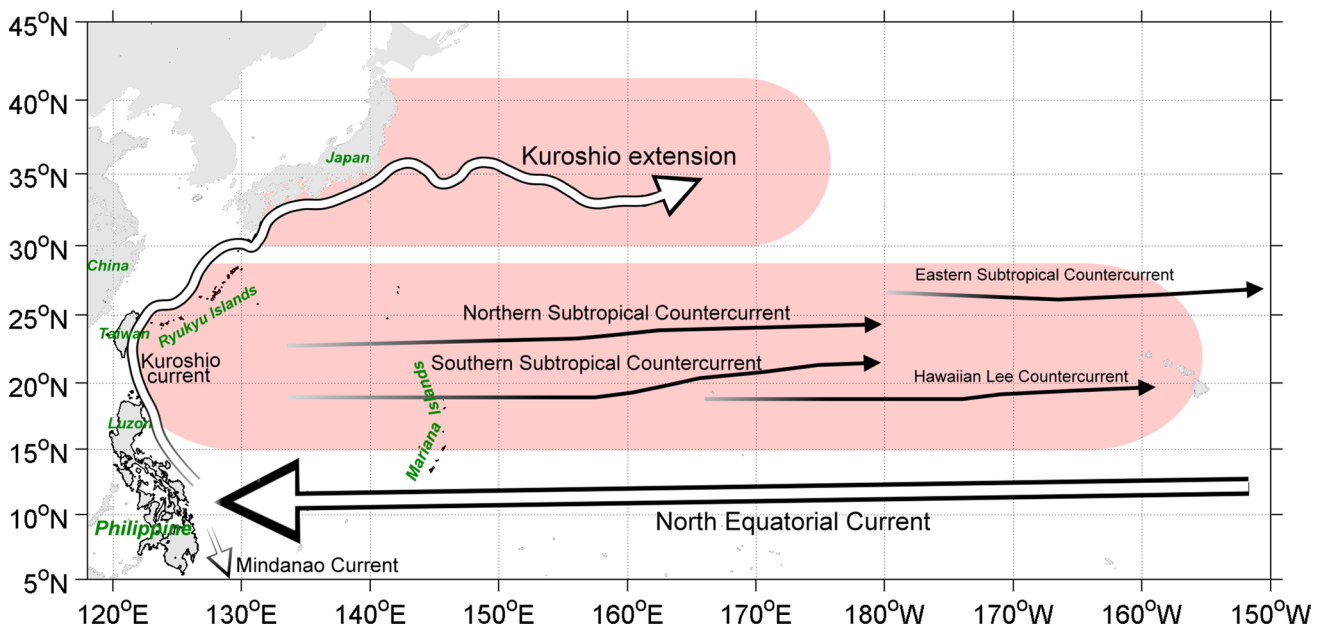


**Fig. 1** Schematic current patterns and two zones with strong eddy kinetic energies (*shaded*) in the western North Pacific Ocean, based on Kida et al. (2015)

22°N–24°N (northern STCC), and 24°N–27°N (eastern STCC) in the western North Pacific. The Hawaiian Lee Countercurrent and southern STCC have similar spatial structures, flowing eastward along 19.5°N against the broad westward North Equatorial Current (Kobashi and Kawamura 2001; Qiu and Chen 2013).

Mesoscale eddies are one of the dominant phenomena in the upper ocean. Petersen et al. (2013) investigated the three-dimensional structures of eddies in global oceans via numerical modeling, and they concluded that nearly one-third of the eddies reach a depth of at least 1,000 m. Furthermore, 97% of eddies with a minimum lifespan of 4 weeks extend to the surface, enabling the detection of these eddies from the sea surface. Thus, eddies can be effectively mapped using high-precision sea level data acquired through satellite altimeters. Using merged altimetry data derived from multi-satellite altimeters, Chelton et al. (2011) demonstrated that eddies propagate westward mostly with the phase speed of long baroclinic Rossby waves and are generated nearly everywhere in the global ocean. The size and energy levels of eddies can also vary in different oceans depending on latitude, ocean stratification, and bottom topography (Isern-Fontanet et al. 2006; Chelton et al. 2011). Mesoscale eddies in the Kuroshio and Kuroshio Extension regions result in the transportation of mass, heat, momentum, and salinity in the Subtropical Gyre (Ebuschi and Hanawa 2001). Moreover, westward-propagating eddies reaching the western boundary current interact with the Kuroshio. The effect of cyclonic eddies on the Kuroshio is entirely different from that of anticyclonic eddies.

In contrast to cyclonic eddies, anticyclonic eddies can accelerate the Kuroshio and contribute to Kuroshio water flow bypassing the Luzon Strait (Kuo and Chern 2011). In addition, eddies modulate the volume transport and path of the Kuroshio (Yang et al. 1999; Johns et al. 2001; Sheu et al. 2010). The mean transport of the Kuroshio is approximately 21.5 Sv ( $1 \text{ Sv} = 10^6 \text{ m}^3 \text{ s}^{-1}$ ), as concluded on the basis of mooring observations conducted in the east of Taiwan; the transport of the Kuroshio reveals a nearly 100-day fluctuation with an amplitude of 6–12 Sv because of the effect of westward-propagating eddies (Zhang et al. 2001).

The western North Pacific comprises two well-defined zonal bands of high eddy kinetic energy (EKE), to which all oceanic motions that deviate from the mean state contribute, including eddies, jet meandering, wave, and jet instability (Waterman et al. 2011). One of these zonal bands is the Kuroshio Extension. The other band is located in the subtropical region between 16°N and 28°N (shaded in Fig. 1) and extends zonally from the east of Taiwan Island and Luzon Island to the Hawaiian Islands (Qiu 1999). This zonal band occupies the central latitudes of the North Pacific Subtropical Gyre and is characterized by the presence of eastward surface flows, the STCCs. Although previous studies have indicated strong EKE in the STCC region, STCCs become obscure to the west and disappear to the west of 130°E, possibly due to eddies. Therefore, how these eddies propagate west of 130°E and intrude into the Kuroshio requires clarification.

Satellite altimeter data are a powerful tool for monitoring the changes of mesoscale eddies in oceans worldwide

and investigating the relationship between eddies and the background mean flow. Hwang et al. (2004) analyzed mesoscale eddies to the east of Taiwan Island using the TOPEX/Poseidon (T/P) data alone, and they found that most eddies over the northern STCC propagate westward along 22°N–24°N to reach the Kuroshio. Eddies propagate westward at a speed of 7.2 cm s<sup>-1</sup> and intensify to the west of the Mariana Islands (Yang et al. 2013). However, the mesoscale variability constructed from the T/P data alone cannot be resolved because of the excessively coarse ground track spacing of the T/P orbit (Chelton et al. 2011). In particular, the effect of eddies on the Kuroshio has rarely been discussed in the STCC region of the subtropical western North Pacific (e.g., Lien et al. 2014; Tsai et al. 2015).

The main purposes of the study reported in the present paper were to clarify hot spots where eddies frequently intrude into the Kuroshio regime and to investigate why those hotspot regions tend to concentrate eddies. To achieve these aims, a sea surface height (SSH)-based eddy identification algorithm was used in this study. The rest of this paper is organized as follows. Section 2 describes the satellite data and eddy data set and defines the SSH-based eddy identification algorithm. Section 3 presents the results of statistical analysis based on the eddy trajectory data set. Section 4 analyzes the factors resulting in concentrated regions of eddy arrivals on the eastern side of the Kuroshio path. Finally, a summary is provided in Sect. 5.

## 2 Data and methodology

### 2.1 Satellite altimeter data

The satellite altimeter sea level anomaly (SLA) and absolute dynamic topography (ADT) data used in this study were provided by Archiving, Validation and Interpretation of Satellite Data in Oceanography (AVISO), with support from the Centre National d'Études Spatiales (CNES) in France. The ADT is defined as the sea surface height above the geoid and is obtained by summing the SLA and the mean dynamic topography (MDT). Briefly, a homogeneous and intercalibrated SLA data set was computed with respect to a 20-year mean (1993–2012) of the SSH. Gridded SLA maps constructed by merging ERS-1/2, TOPEX/Poseidon, Jason-1/2, and Envisat altimeters were geophysically and meteorologically corrected (tides, ionosphere, atmospheric pressure correction, wet troposphere, and dry troposphere) and interpolated onto Mercator grids with a horizontal resolution of 1/4°. In addition, the MDT was derived from a geoid model on the basis of 4.5-year Gravity Recovery and Climate Experiment (GRACE) data and combined with 16 years of in situ measurements [drifting buoys, Argo floats, and conductivity–temperature–depth

(CTD) profilers], altimetry, and wind stress data. The CNES-CLS09 MDT is highly consistent with in situ observations, especially for the western boundary currents (Maximenko et al. 2009; Rio et al. 2011). These altimetry products cover the period from October 1992 to the present time (<http://www.aviso.oceanobs.com/en/data/products.html>).

### 2.2 Trajectories of mesoscale eddies

Several automated eddy algorithms have been developed to detect and track ocean eddies. Chelton et al. (2011) applied an SSH-based eddy identification algorithm to study ocean eddies. This method has been widely used in numerous studies (e.g., Escudier et al. 2016), and allows good control over the eddy trajectory. For a more detailed description, a comparative analysis of several automated eddy algorithms was conducted by Souza et al. (2011). The eddy-tracking data set, collected from October 1992 to April 2012, is available online (<http://cioss.coas.oregonstate.edu/eddies>), and the present study used the processed data set to investigate where eddies frequently intrude into the Kuroshio. We now simply describe the methodology used by Chelton et al. (2011).

The eddy trajectories described herein are applied to the 19.5-year records of SSH fields at a horizontal resolution of 1/4°, affording sufficient spatial resolution to identify and track mesoscale eddies. Since large-scale SSH variations often mask the subtle signatures of eddies, the SSH fields are first filtered by applying a high-pass filter, removing coherent signals with wavelength scales greater than 10° (latitude) by 20° (longitude), so as to distinguish eddies from other features. An eddy can be intuitively defined as an isolated rotary structure with localized variations in sea levels, and can be identified on the basis of the closed contours of the filtered SSH fields. As described in detail in Appendix B of the publication by Chelton et al. (2011), this method can reduce the influence of large-scale variability.

For eddy centers detected from SSH fields at each seven-day time step, an automated tracking method is applied to determine the path of each eddy. For eddies identified at time step  $t$ , eddies identified at the next time step  $t + 1$  are explored by finding the closest eddy center with the same sign of relative vorticity within a search radius of 150 km, but the western eddy search region extends according to the phase speed of long Rossby waves. In addition, to reduce the risk of spurious eddies arising from SSH-field noise, eddies tracked through this method with a lifespan of <4 weeks are eliminated, because the satellite altimetry data of the AVISO Reference Series are constructed by applying a 35-day  $e$ -folding timescale of a Gaussian covariance function in an objective analysis procedure. Additional details on the SSH-based eddy identification algorithm can be found in Chelton et al. (2011).

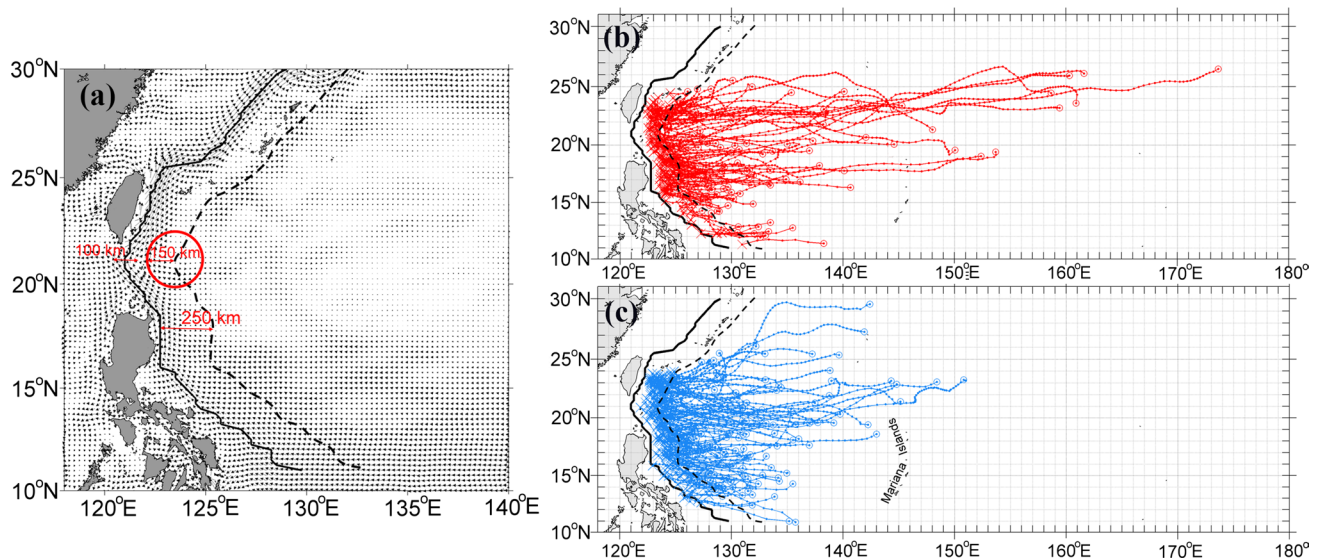


**Fig. 2** a Mean geostrophic current field from October 1992 to April 2012. The *solid line* and the *dashed line* denote the mean axis of the Kuroshio and the eddy-effect line, respectively. The *red circle* repre-

sents a sketch of an eddy. Map of backtracked trajectories of anticyclonic (b) and cyclonic (c) eddies. The *circles* and *crosses* represent the locations of eddy generation and termination, respectively

### 3 Results

#### 3.1 Statistical features of eddy intrusion

The mean axis (solid line in Fig. 2a) of the Kuroshio maximum velocity at the sea surface was derived from long-term average ADT fields from October 1992 to April 2012. The mean width of the Kuroshio is approximately 100 km (Liang et al. 2003), and the maximum radius of mesoscale eddies can exceed 150 km (Chelton et al. 2011). This study observed the distribution of eddies before their interaction with the Kuroshio. On the basis of the preceding hypotheses, we assumed that eddies are affected by the northward-flowing Kuroshio within the 250-km range close to the east side of the Kuroshio; thus, the eddy-effect line (dashed line in Fig. 2a) was used to discern the locations of the eddies before they were affected by the Kuroshio. During the process of intruding into the western side of the eddy-effect line (between the solid line and the dashed line in Fig. 2a), eddies potentially impinge on and interact with the Kuroshio. In the following analysis, we will focus on the eddies which can propagate across the eddy-effect line to the Kuroshio regime, but eddies generated around the Kuroshio axis (the western side of the dashed line in Fig. 2a) were not considered in this study.

The trajectories of anticyclonic and cyclonic eddies with lifespans  $\geq 4$  weeks are presented in Fig. 2b, c. In total, the automated procedure detected 315 eddies crossing over the eddy-effect line, consisting of 138 anticyclonic eddies and 177 cyclonic eddies. More than 95% of the 315 eddies analyzed herein (Fig. 2) were generated in

the ocean west of the Mariana Islands. Notably, no eddies impinge on the Kuroshio from 25°N to 30°N, as indicated in Fig. 2b, c. Eddies almost dissipate near the Ryukyu Islands before they propagate across the eddy-effect line, which implies that the Kuroshio on the western side of the island chain could be shielded from the direct intrusion of eddies. Most eddies are easily blocked by the island chain or the Kuroshio and then dissipate. However, some eddies, generated around the Kuroshio axis (not shown here), may cross the Luzon Strait and enter the South China Sea (Sheu et al. 2010; Zheng et al. 2011; Hu et al. 2012).

Census statistics of properties when eddies propagate across the eddy-effect line are shown in Fig. 3. The eddy length scale can be characterized using the speed-based radius; this parameter is defined as the radius of a circle with an area equal to that enclosed by the SSH contour with maximum circum-average speed (Chelton et al. 2011, Appendix B.3). The mean scale of eddies investigated in this study was found to be approximately 130 km, and the average maximum rotation speed was observed to be approximately  $30 \text{ cm s}^{-1}$ . The latitude of eddy-intrusion location through time is illustrated in Fig. 3a. Eddies clearly actively intrude into the Kuroshio regime between 14°N and 24°N. Furthermore, the latitudes of eddies crossing the eddy-effect line were estimated. Histograms of the crossing latitudes are illustrated in Fig. 3b, indicating that the eddies are concentrated in the regions at 18°N–19°N and 22°N–23°N. These two active bands of eddy intrusion were further confirmed by the period of eddy intrusion, defined as the time interval between two consecutive eddies while

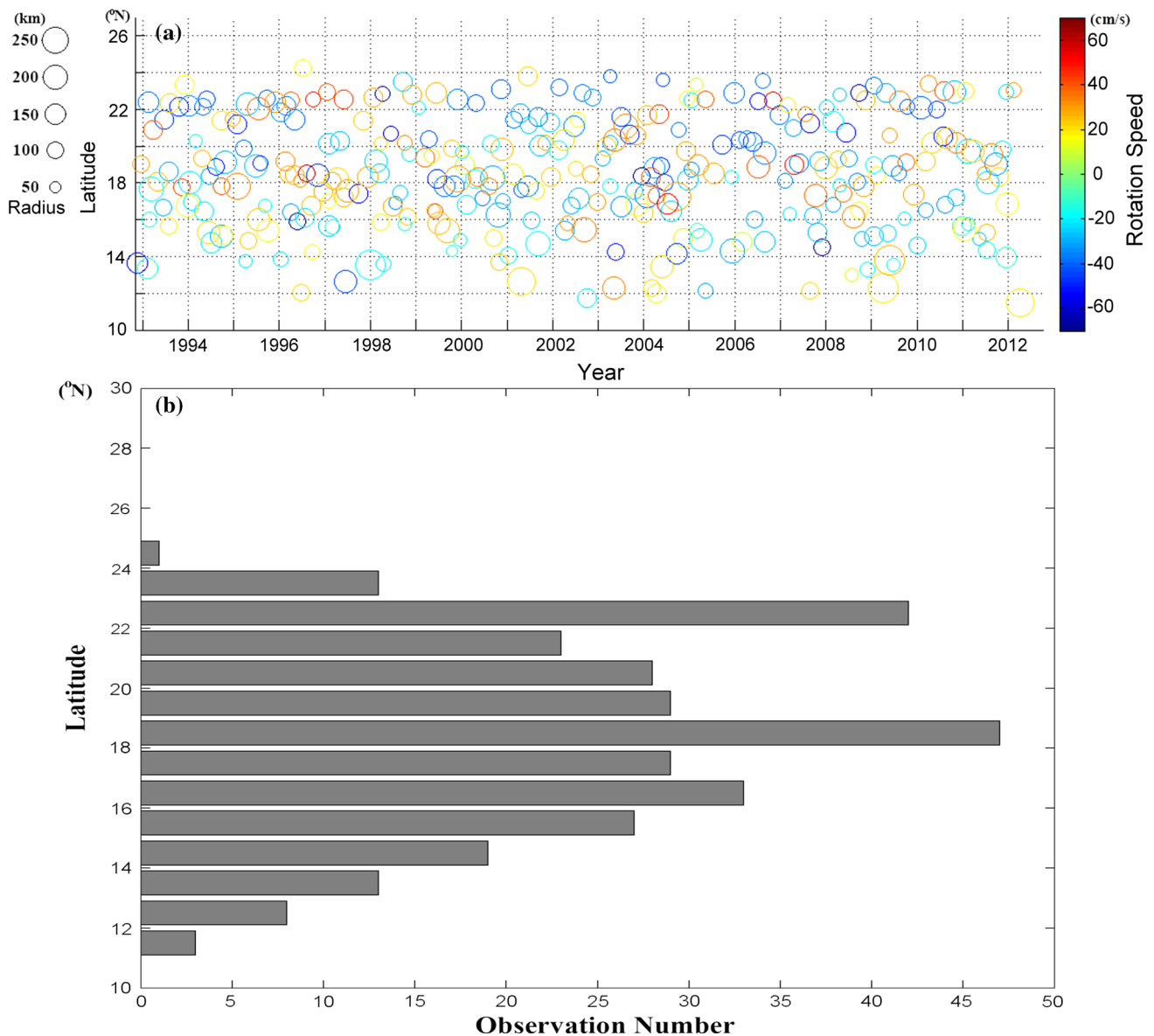


**Fig. 3** **a** Census statistics of eddy properties when they cross the eddy-effect line (dashed line in Fig. 2a). The size of the circle on the left denotes the eddy radius. The color scale on the right side of panel **a** displays the maximum rotation speed ( $U_R$ ) within eddies. Positive

and negative values indicate anticyclonic and cyclonic eddies, respectively. **b** Histogram of latitudes of eddies as they cross the eddy-effect line

crossing the eddy-effect line. Figure 4a illustrates that eddies intrude into the Kuroshio regime through these two latitude bands more frequently than they do through other latitudes. The average intrusion periods (approximately  $146 \pm 62$ -day period at  $18^\circ\text{N}$ – $19^\circ\text{N}$  and approximately  $165 \pm 46$ -day period at  $22^\circ\text{N}$ – $23^\circ\text{N}$ ) are close to the fluctuation of the Kuroshio estimated from mooring array data (approximately 70- to 200-day periods; Zhang et al. 2001), oceanographic radar data (10- to 240-day periods; Ichikawa et al. 2008), and current fields of a coastal model (70- to 150-day periods; Lee et al. 2013). These results imply that

eddies frequently intrude into the Kuroshio regime not only through  $22^\circ\text{N}$ – $23^\circ\text{N}$  (Hwang et al. 2004) but also through  $18^\circ\text{N}$ – $19^\circ\text{N}$ .

To understand the interaction time between eddies and the Kuroshio, we estimated the time interval between first encountering the eddy-effect line and finally dissipating in the Kuroshio regime. The latitudinal variation of the interaction time (Fig. 4b) illustrates that the eddies exist longer in the Kuroshio regime through the latitude bands  $18^\circ\text{N}$ – $19^\circ\text{N}$  and  $22^\circ\text{N}$ – $23^\circ\text{N}$ , and the average interaction time was found to be  $33 \pm 10$  days and  $45 \pm 17$  days,

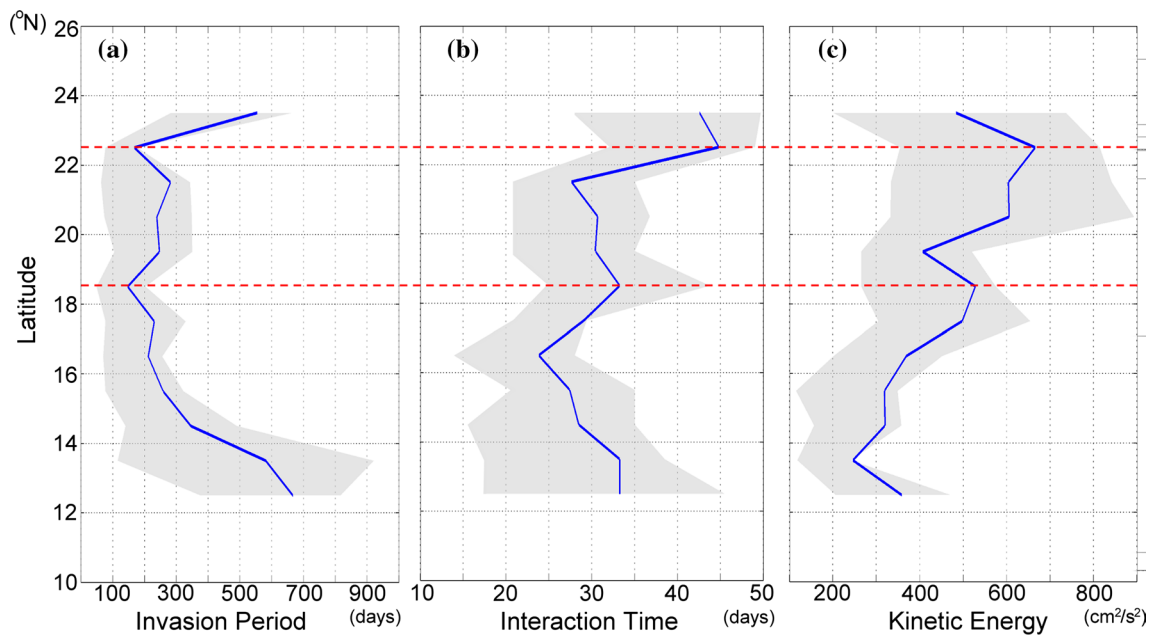


**Fig. 4** The latitudinal variations in **a** the intrusion period, **b** the interaction time, and **c** the kinetic energy were estimated for each degree of latitude. Mean value is shown by a blue line, and gray shading

indicates the interquartile range. Red dashed lines denote the two latitude bands, 18°N–19°N and 22°N–23°N

respectively. This result can be explained by considering the kinetic energy (Fig. 4c), defined as  $U_R^2/2$ , where  $U_R$  is the maximum rotation speed within the eddy. Eddies with high rotation speeds can strongly maintain their shape during propagation (Chelton et al. 2011). When the kinetic energy is greater, the interaction time between an eddy and the Kuroshio is potentially longer.

### 3.2 Two hot spots of eddy intrusion

As eddies cross the eddy-effect line, they are concentrated at latitudes of 18°N–19°N and 22°N–23°N, where eddies frequently intrude into the Kuroshio regime and survive for a long time within it (these are hereafter referred to as the “hot spots” of eddy intrusion). Herein, we focus on the trajectories of eddies intruding into the Kuroshio through the two hot spots as follows. A notable feature of the trajectories shown in Fig. 5a,c is westward propagation with little meridional deflection. As the trajectory lengthens, the deflection becomes more visible. Cyclonic eddies exhibit poleward deflection; anticyclonic eddies, by contrast, exhibit equatorward deflection (Morrow et al. 2004; Chelton et al. 2007). This deviation phenomenon may be explained by  $\beta$ -effect theory (Cushman-Roisin et al. 1990). The deflection angle is theorized to be approximately 2° near 22°N, which is in agreement with most eddy deflections in our study region. However, a few eddies (such as cyclonic eddies at latitudes higher than 25°N in Fig. 5a,b) are mainly affected by other factors (as described in

Sect. 4.2). In addition, we would like to clarify where these eddies came from. Histograms of the origins of the eddies concentrated within the two hot spots are illustrated in Fig. 5b,d. Nearly 80% of the eddies concentrated within the southern latitude band (18°N–19°N) originate from the 17°N–20°N band. Similarly, nearly 50% of the eddies concentrated within the northern latitude band (22°N–23°N) originate from the 21°N–24°N band. Most of the eddies originate from similar zonal bands. Nevertheless, the trajectories are complex, and can be affected by noise from the SSH fields, eddy–eddy interactions, and eddy–mean flow interactions (Chelton et al. 2011).

## 4 Discussion

### 4.1 Effects of two eastward branches of the STCCs

Kobashi et al. (2006) revealed that the STCCs comprise three eastward jets: the southern STCC centered along approximately 19°N–21°N from 130°E to 180°, the northern STCC centered along approximately 22°N–25°N from 130°E to 180°, and the eastern STCC north of the Hawaiian Islands centered along nearly 26°N from 175°E to 160°W. A map of the geographical distribution of the average zonal current in 1/4°-square regions is presented in Fig. 6a, clearly indicating that the latitudes of two eastward currents, located at 17°N–20°N (the southern STCC) and 22°N–25°N (the northern STCC), are consistent with the

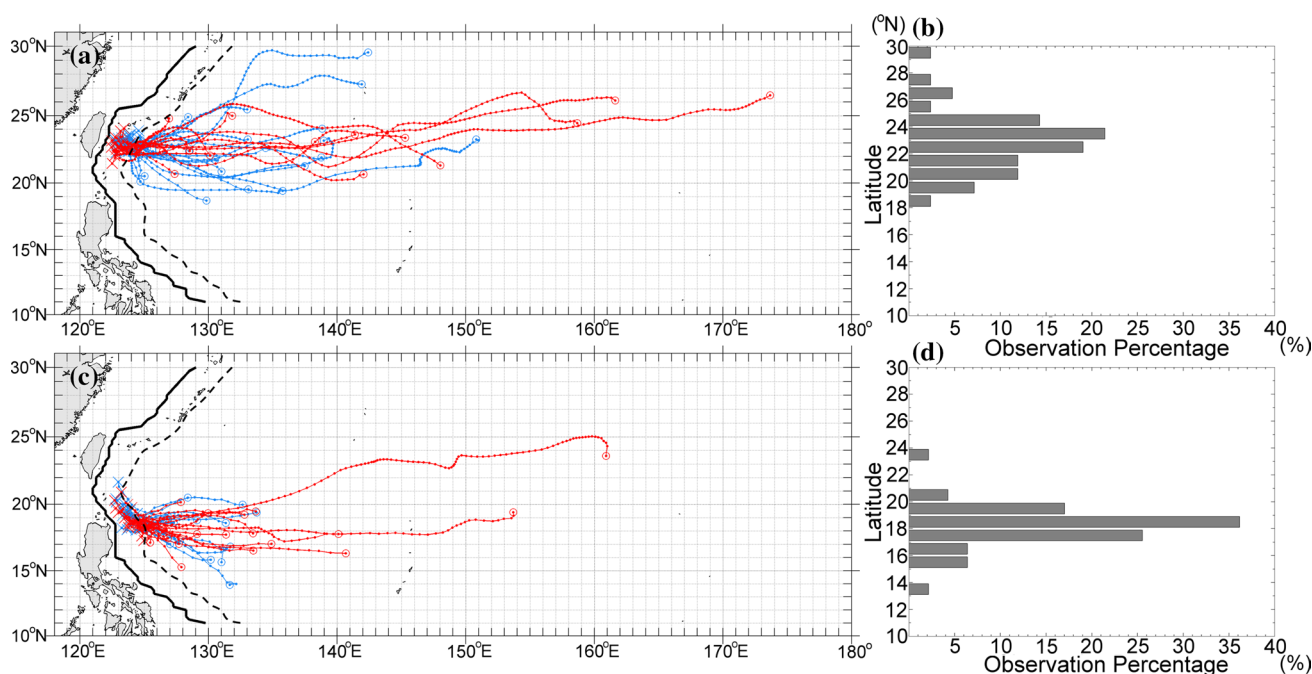


**Fig. 5** a, c Eddy trajectories concentrated at a 22°N–23°N and c 18°N–19°N. The red and blue lines correspond to anticyclonic and cyclonic eddies, respectively. Circles and crosses represent the locations of eddy generation and termination, respectively. Dots represent

eddies detected from SSH fields with a 7-day time step. b, d Histograms of origin locations for the eddies intruding into the Kuroshio through the two hot spots at b 22°N–23°N and d 18°N–19°N

two hot spots of eddy intrusion (Fig. 3b) and the latitudes of origin of the eddies (Fig. 5b, d).

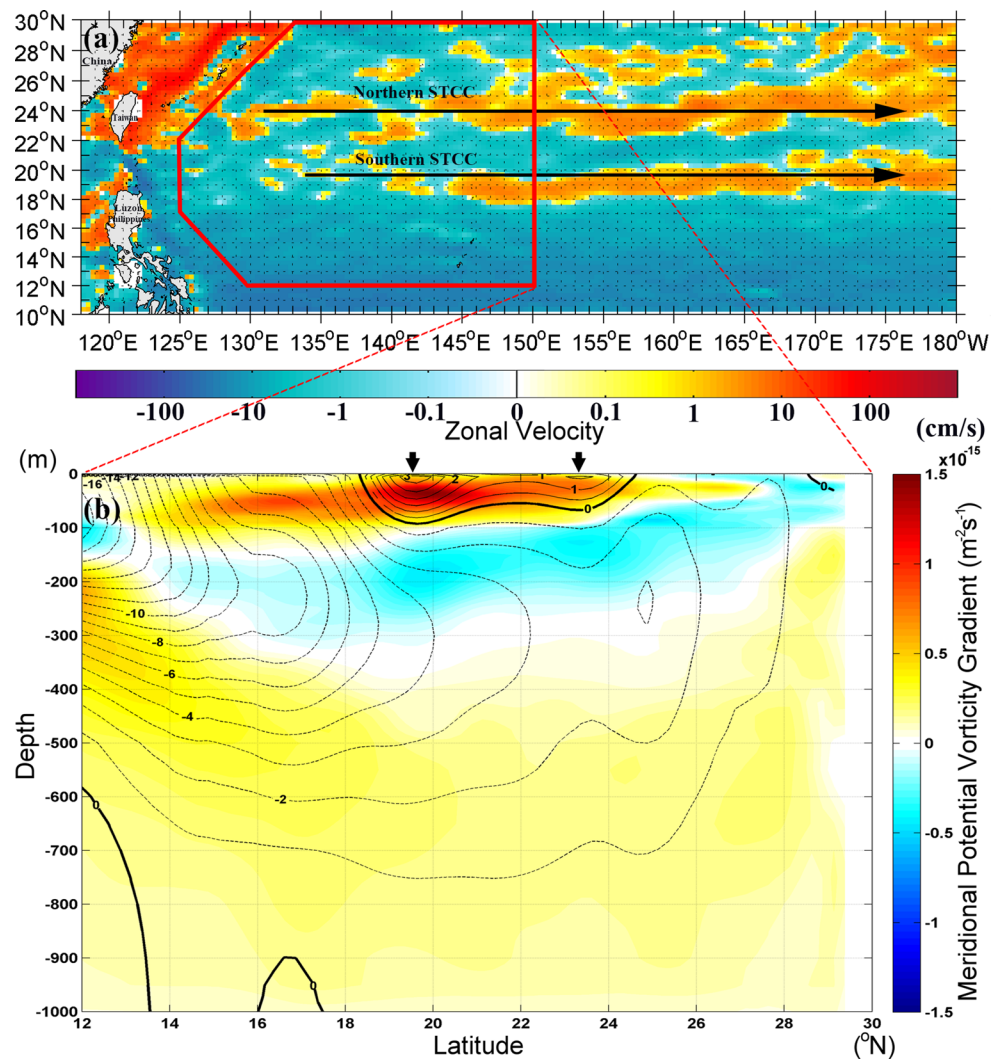
We used the World Ocean Atlas 2013 version 2 data set of temperature and salinity to calculate the geostrophic velocity (relative to 1000 m). Figure 6b shows the annual mean profile of the zonal geostrophic velocity averaged from 125°E to 150°E (Fig. 6a, red box). In the meridional section, two cores of eastward currents occur in the upper ocean at around 19°N and 23°N (Fig. 6b, black arrows). The wind-driven westward current, the North Equatorial Current, exists below the upper layer. The bounding depth is approximately 100 m. Kobashi and Kawamura (2002) and Qiu (1999) used altimeter data to investigate the relationships between the seasonal modulation of STCCs and the EKE, and reported that eddies are generated by the subtropical front associated with an eastward countercurrent. Strong vertical shear and a small stratification ratio increase the potential baroclinic instability. According to the method of Kobashi and Kawamura (2002), the potential vorticity (PV), defined as  $(f/\rho)(\partial\sigma_\theta/\partial z)$ , is derived from the hydrographic data of WOA13, where  $f$  is the Coriolis parameter,  $\rho$  is the density, and  $\sigma_\theta$  is the potential density. From the vertical section of the meridional PV gradient (color shading in Fig. 6b), the meridional PV gradient is positive in the upper 100 m in the near-surface eastward STCCs; by contrast, it is negative in the subsurface layer at approximately 100–300 m. Reversing the sign of the meridional

PV gradient in the vertical direction results in baroclinic instability, which is a vital energy source for eddy generation in the western North Pacific Subtropical Gyre (Qiu 1999; Kobashi and Kawamura 2002). Qiu and Chen (2013) reported that eddy activity modulation is highly dependent on the change in the upper-ocean eastward shear inside the western North Pacific Subtropical Gyre. These results imply that the eddies that frequently intrude into the Kuroshio through the two hot spots (Fig. 5) mainly originate from the southern STCC and the northern STCC. Eddies generated near 19°N and 23°N may become trapped along the two axes of the STCCs. Although the STCCs become obscure to the west and disappear to the west of 130°E, most of the eddies intrude into the Kuroshio regime along same latitude bands.

#### 4.2 Effect of the Ryukyu Islands and the recirculation gyre

The Ryukyu Islands, which include numerous islands and islets, are northeast of Taiwan (Fig. 7). This island chain is arranged in a curved row extending to 24°N (east of Taiwan) and forms the border between the East China Sea and the western North Pacific. The Kuroshio flows northeastward through the Okinawa Trough and is shielded from the westward-propagating eddies by the island chain; nevertheless, eddies can still indirectly result in delayed variations

**Fig. 6** **a** Map of average zonal geostrophic currents derived from ADT maps from October 1992 to April 2012. A logarithmic color scale is used to highlight the STCCs. Positive values and negative values indicate eastward and westward, respectively. **b** Cross-section profiles of meridional potential vorticity (PV) gradient (colors) and zonal geostrophic velocity (contours) relative to 1000 m. In panel **b**, the two parameters are derived from the annual mean hydrographic data and averaged between 125°E and 150°E (red box in panel **a**). Contour intervals are  $1 \text{ cm s}^{-1}$  (dashed contours) for westward currents and  $0.5 \text{ cm s}^{-1}$  (solid contours) for eastward currents. Black arrows indicate the locations of the two STCC cores

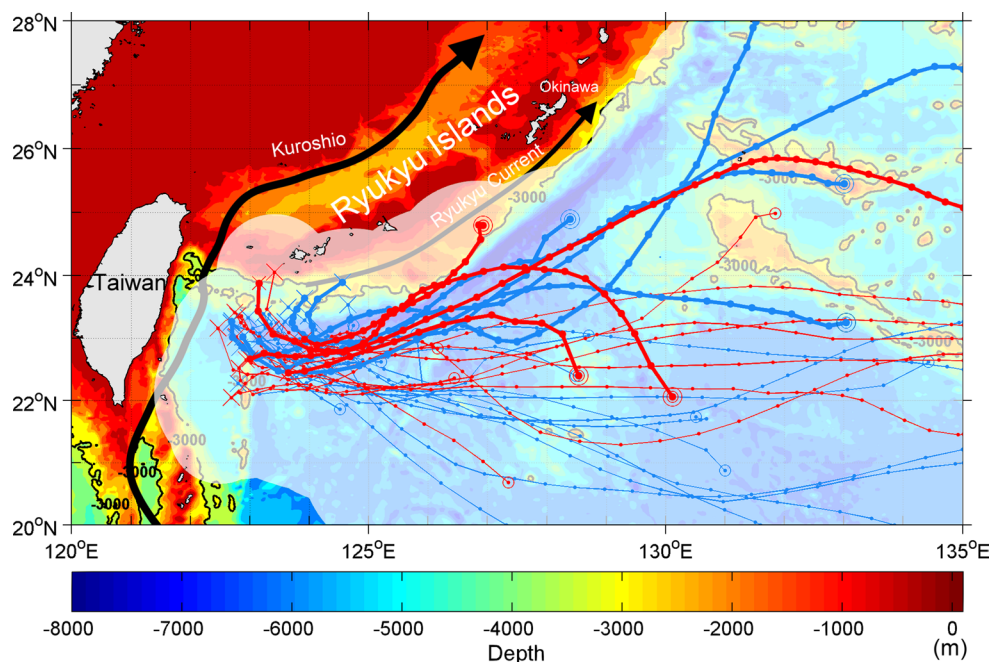


of the Kuroshio volume transport (Andres and Cenedese 2013). In contrast to the Kuroshio, the Ryukyu Current, which flows with a subsurface maximum northeastward along the eastern side of the island chain (Fig. 7), is directly affected by impinging eddies. The intensity of the Ryukyu Current is generally weaker than that of the Kuroshio. Some eddies are strong enough to reverse the direction of the Ryukyu Current pattern near Okinawa, one of the Ryukyu Islands (Zhu et al. 2004).

Figure 7 shows the bathymetry around the Ryukyu Islands as well as eddy trajectories along with their areas of influence. The area of influence was defined as the region within the speed-based radius of each eddy. A significant feature of the eddy trajectories is that most eddies approaching the Ryukyu Islands (Fig. 7, thick lines) propagate southwestward along the island chain. To strengthen this argument, eddies with long lifespans ( $\geq 4$  weeks) in our study region were considered, and the eddy-propagation velocity was averaged during the study period. From the

mean velocity field shown in Fig. 8, a tendency for nearly due-west propagation is apparent in region  $Z_A$  (Fig. 8a). While approaching the island chain, the eddy-propagation velocity shifts southwestward in region  $Z_B$  or decreases to zero in region  $Z_C$ . This implies that some eddies, such as those illustrated in Fig. 7, possibly propagate southwestward when approaching the Ryukyu Islands. The results reveal that eddies originating at high latitudes (Fig. 7) do not dissipate when approaching the Ryukyu Islands but instead propagate southwestward along the island chain. Moreover, because the Ryukyu Islands are arranged in a curved row extending to 24°N, and because the mean eddy radius is approximately 150 km, eddies propagating along the island chain are concentrated within 22°N–23°N. Therefore, the histogram of eddy origins (Fig. 5b) is skewed more to the higher latitudes than to the latitude of the northern hot spot (22°N–23°N). Zhai et al. (2010) produced an eddy energy map showing a more significant sink of eddy energy east of Taiwan than that to the east of the

**Fig. 7** Bathymetry around the Ryukyu Islands (*shaded*) and trajectories of eddies concentrated within 22°N–23°N. *White shadows* are areas of influence drawn on the basis of eddy radius. Trajectories with a radius of influence that includes the island chain are *highlighted with thick lines*; the mean positions of the Kuroshio maximum velocity and the Ryukyu Current are marked by *black arrows*



Ryukyu Islands. This pattern indirectly indicates that some westward-propagating eddies might not dissipate when they approach the Ryukyu Islands, but continue to propagate southwestward along the curved island chain toward the east of Taiwan. Additionally, eddies are affected by the northward Kuroshio flow on the western side of the eddy-effect line ( $Z_D$  in Fig. 8a); thus, eddy propagation shifts northwestward and then the eddies dissipate on the east of Taiwan.

The southward propagation can be explained by simply decomposing the velocity vectors. The westward velocity can be divided into two components, the along-coast velocity ( $U_A$ ) and cross-coast velocity ( $U_C$ ), as illustrated in the top right panel of Fig. 8.  $U_C$  would be weakened by the island chain (Fig. 8c), and  $U_A$  would drive eddies to propagate southwestward along the Ryukyu Islands, as shown in Fig. 8d. One can see that the along-coast (southwestward) velocity is more influential in  $Z_B$  than in the other regions. The southward propagation may also be explained by the bathymetry-induced  $\beta$ -effect. Eddies propagate along an island chain with the shallower region on their right side in the Northern Hemisphere (Smith and O'Brien 1983; Cushman-Roisin et al. 1990). In addition, an anticyclonic recirculation gyre exists to the east of the Ryukyu Islands, and extends southwestward from Japan (Nakamura et al. 2007; Thoppil et al. 2016). The southwestward recirculation flow may drive eddies to propagate southwestward. Nevertheless, the effect of eddy–eddy (eddy–mean flow) interaction on eddy propagation cannot be ignored; therefore, additional investigations are required to completely understand the movement processes during the lifespan of an eddy.

## 5 Summary

In this study, we used satellite altimeter sea-level data to investigate the statistical features of eddies which intrude into the Kuroshio regime near the Luzon–Taiwan eastern coast. We applied an identification method to identify and trace eddies. Using an eddy-tracking data set from October 1992 to April 2012, we quantified the distribution and characteristics of eddies approaching the Kuroshio. The automated procedure detected 315 eddies crossing the eddy-effect line and intruding into the Kuroshio regime, comprising 138 anticyclonic eddies and 177 cyclonic eddies. More than 95% of the eddies are generated in the ocean west of the Mariana Islands. The length scale and rotation speed of the eddies in the study region were found to be approximately 130 km and  $30 \text{ cm s}^{-1}$ , respectively. The eddies intrude into the Kuroshio regime at 18°N–19°N ( $146 \pm 62$ -day period) and 22°N–23°N ( $165 \pm 46$ -day period) more frequently than they do at other latitudes. Similarly, the interaction time between the eddies and the Kuroshio at these two latitude bands ( $33 \pm 10$  days at 18°N–19°N and  $45 \pm 17$  days at 22°N–23°N) were observed to be longer than those at other latitudes. In addition, the Kuroshio from 25°N to 30°N is shielded from the direct intrusion of eddies by the Ryukyu Islands.

Tracking results show that the concentration of eddies within the two hot spots of eddy intrusion are governed by the northern STCC and the southern STCC. Reversing the sign of the meridional PV gradient from the near-surface (approximately  $1 \times 10^{-15} \text{ m}^{-2} \text{ s}^{-1}$  in the upper 100 m) to

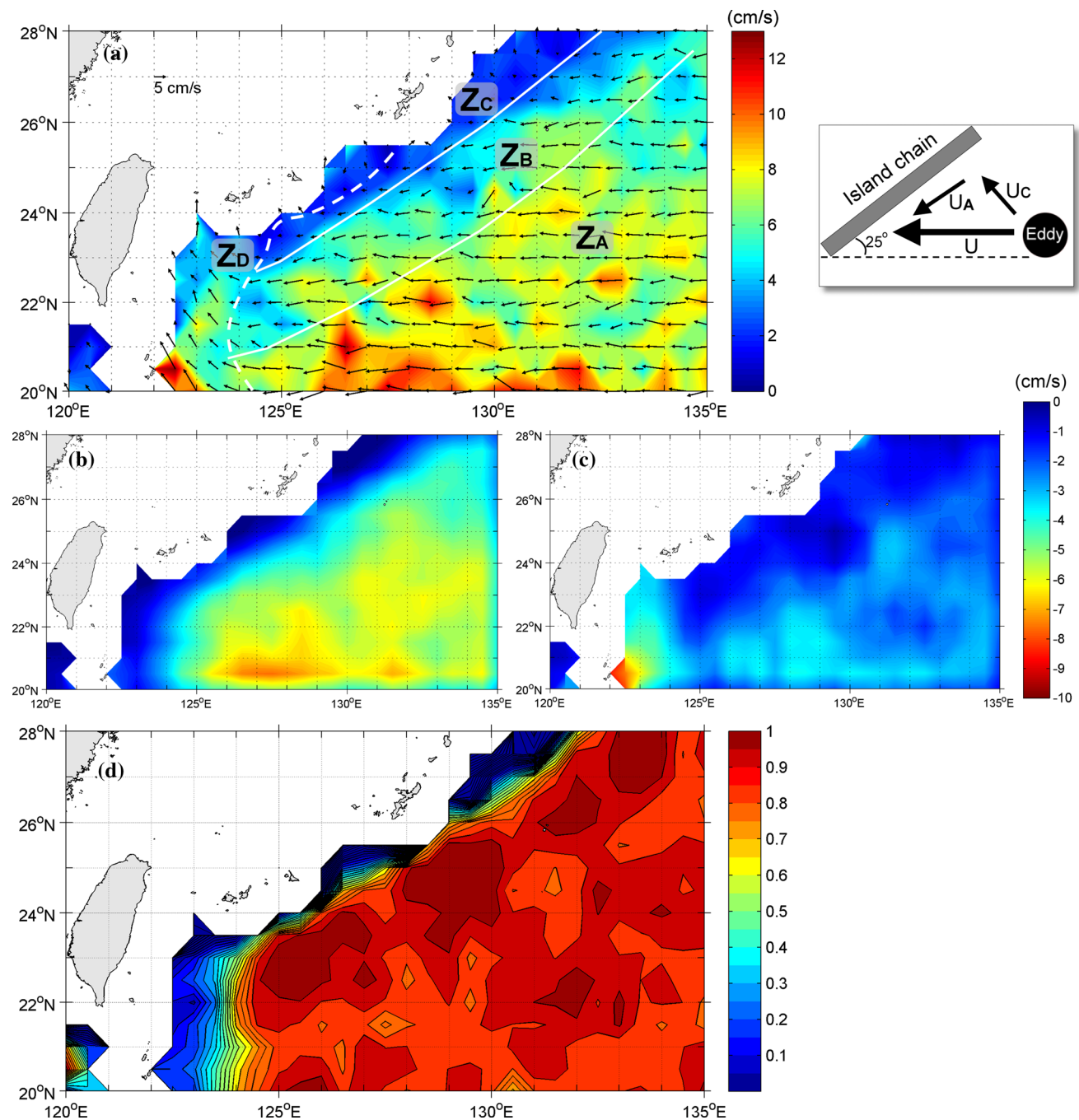


**Fig. 8** **a** Climatological means of eddy propagation velocity vectors and magnitudes (*shaded*) from October 1992 to April 2012. The *dashed line* denotes the eddy-effect line. The *white lines* denote the boundaries of regions Z<sub>A</sub>–Z<sub>D</sub>. A sketch of the island chain and an approaching eddy are shown in the *top right* of the figure. Here, *U* is

the eddy velocity;  $U_A$  and  $U_C$  are the along-coast component (**b**) and cross-coast component (**c**) of  $U$ , respectively. Negative values indicate southwestward propagation in Fig. 8b or northwestward propagation in Fig. 8c. **d** Map of the southwestward percentage, defined as  $|U_A|/|U_A + U_C|$

the subsurface (approximately  $-5 \times 10^{-16} \text{ m}^{-2} \text{ s}^{-1}$  at 100–300 m depth) provides a vital energy source for eddy generation. Therefore, mesoscale eddies are easily generated and possibly trapped within the two STCC axes. Moreover, eddies are affected by the bathymetry and southwestward

recirculation flows when they approach the Ryukyu Islands, which are arranged in a curved row extending to the east of Taiwan. The velocity fields of eddy propagation indicate that westward eddies possibly continue to propagate southwestward instead of directly dissipating near the

island chain. Eddies move along the Ryukyu Islands toward Taiwan and intrude into the Kuroshio regime. These results indicate that the island chain and the recirculation gyre are other factors that cause the concentration of eddies at 22°N–23°N when they are about to intrude into the Kuroshio regime. Subsequently, eddies were dragged northward while intruding into the Kuroshio regime; northward eddies were blocked by the Ryukyu Islands and dissipated to the east of Taiwan, which is a major eddy dissipation region in the subtropical western North Pacific.

According to our study findings, we suggest that eddies frequently intrude into the Kuroshio at two latitude bands, namely 18°N–19°N and 22°N–23°N, in the subtropical western North Pacific. The concentration of eddies within the two hot spots of eddy intrusion is attributed to two factors, namely the STCCs and the Ryukyu Islands. These results may imply a high probability of the Kuroshio volume transport being modulated through these two hot spots of eddy intrusion. Eddies can affect the variation of the Kuroshio path east of Taiwan Island and Luzon Island, especially to the east of the Luzon Strait, which is a water gate between the western North Pacific and the South China Sea.

**Acknowledgements** The authors appreciate all of the constructive comments from reviewers. The altimeter products used in this study were produced by Ssalto/Duacs and distributed by AVISO, with support from CNES (<http://www.aviso.oceanobs.com/duacs/>). The eddy data set was produced by Dudley B. Chelton and Michael G. Schlax (<http://cioss.coas.oregonstate.edu/eddies/>). Cheng and Ho were supported by the National Science Council of Taiwan (NSC 101-2611-M-019-003 and NSC 102-2611-M-019-011). Cheng and Hu were supported by the National Natural Science Foundation of China (U1405233).

## References

- Andres M, Cenedese C (2013) Laboratory experiments and observations of cyclonic and anticyclonic eddies impinging on an island. *J Geophys Res Oceans* 118(2):762–773. doi:10.1002/jgrc.20081
- Chelton DB, Schlax MG, Samelson RM, de Szoeke RA (2007) Global observations of large oceanic eddies. *Geophys Res Lett* 34:L15606. doi:10.1029/2007GL030812
- Chelton DB, Schlax MG, Samelson RM (2011) Global observations of nonlinear mesoscale eddies. *Prog Oceanogr* 91(2):167–216. doi:10.1016/j.pocean.2011.01.002
- Cushman-Roisin B, Tang B, Chassignet EP (1990) Westward motion of mesoscale eddies. *J Phys Oceanogr* 20(5):758–768. doi:10.1175/1520-0485(1990)020<0758:wmome>2.0.co;2
- Ebuchi N, Hanawa K (2001) Trajectory of mesoscale eddies in the Kuroshio recirculation region. *J Oceanogr* 57(4):471–480. doi:10.1023/A:1021293822277
- Escudier R, Renault L, Pascual A, Brasseur P, Chelton D, Beuvier J (2016) Eddy properties in the Western Mediterranean Sea from satellite altimetry and a numerical simulation. *J Geophys Res Oceans* 121(6):3990–4006. doi:10.1002/2015JC011371
- Hasunuma K, Yoshida K (1978) Splitting of the subtropical gyre in the western North Pacific. *J Oceanogr Soc Jpn* 34(4):160–172. doi:10.1007/BF02108654
- Hu J, Zheng Q, Sun Z, Tai C-K (2012) Penetration of nonlinear Rossby eddies into South China Sea evidenced by cruise data. *J Geophys Res Oceans*. doi:10.1029/2011JC007525
- Hwang C, Wu C-R, Kao R (2004) TOPEX/Poseidon observations of mesoscale eddies over the Subtropical Countercurrent: kinematic characteristics of an anticyclonic eddy and a cyclonic eddy. *J Geophys Res Oceans* 109:C08013. doi:10.1029/2003JC002026
- Ichikawa K, Tokeshi R, Kashima M, Sato K, Matsuoka T, Kojima S, Fujii S (2008) Kuroshio variations in the upstream region as seen by HF radar and satellite altimetry data. *Int J Remote Sens* 29(21):6417–6426. doi:10.1080/01431160802175454
- Isern-Fontanet J, Garcia-Ladona E, Font J (2006) Vortices of the Mediterranean Sea: an altimetric perspective. *J Phys Oceanogr* 36(1):87–103. doi:10.1175/JPO2826.1
- Johns WE, Lee TN, Zhang D, Zantopp R, Liu C-T, Yang Y (2001) The Kuroshio east of Taiwan: moored transport observations from the WOCE PCM-1 array. *J Phys Oceanogr* 31(4):1031–1053. doi:10.1175/1520-0485(2001)031<1031:TKEOTM>2.0.CO;2
- Kida S, Mitsudera H, Aoki S, Guo X, S-i Ito, Kobashi F, Komori N, Kubokawa A, Miyama T, Morie R, Nakamura H, Nakamura T, Nakano H, Nishigaki H, Nonaka M, Sasaki H, Sasaki YN, Suga T, Sugimoto S, Taguchi B, Takaya K, Tozuka T, Tsujino H, Usui N (2015) Oceanic fronts and jets around Japan: a review. *J Oceanogr* 71(5):469–497. doi:10.1007/s10872-015-0283-7
- Kobashi F, Kawamura H (2001) Variation of sea surface height at periods of 65–220 days in the subtropical gyre of the North Pacific. *J Geophys Res: Oceans* 106(C11):26817–26831. doi:10.1029/2000JC000361
- Kobashi F, Kawamura H (2002) Seasonal variation and instability nature of the North Pacific Subtropical Countercurrent and the Hawaiian Lee Countercurrent. *J Geophys Res Oceans* 107(C11):3185. doi:10.1029/2001JC001225
- Kobashi F, Mitsudera H, Xie S-P (2006) Three subtropical fronts in the North Pacific: observational evidence for mode water-induced subsurface frontogenesis. *J Geophys Res Oceans* 111:C09033. doi:10.1029/2006JC003479
- Kuo Y-C, Chern C-S (2011) Numerical study on the interactions between a mesoscale eddy and a western boundary current. *J Oceanogr* 67(3):263–272. doi:10.1007/s10872-011-0026-3
- Lee I-H, Ko DS, Wang Y-H, Centurioni L, Wang D-P (2013) The mesoscale eddies and Kuroshio transport in the western North Pacific east of Taiwan from 8-year (2003–2010) model reanalysis. *Ocean Dyn* 63(9–10):1027–1040. doi:10.1007/s10236-013-0643-z
- Liang W-D, Tang T, Yang Y, Ko M, Chuang W-S (2003) Upper-ocean currents around Taiwan. *Deep Sea Res Part II* 50(6):1085–1105
- Lien R-C, Ma B, Cheng Y-H, Ho C-R, Qiu B, Lee CM, Chang M-H (2014) Modulation of Kuroshio transport by mesoscale eddies at the Luzon Strait entrance. *J Geophys Res Oceans* 119(4):2129–2142. doi:10.1002/2013JC009548
- Maximenko N, Niiler P, Centurioni L, Rio M-H, Melnichenko O, Chambers D, Zlotnicki V, Galperin B (2009) Mean dynamic topography of the ocean derived from satellite and drifting buoy data using three different techniques. *J Atmos Ocean Technol* 26(9):1910–1919. doi:10.1175/2009JTECHO672.1
- Morrow R, Birol F, Griffin D, Sudre J (2004) Divergent pathways of cyclonic and anti-cyclonic ocean eddies. *Geophys Res Lett*. doi:10.1029/2004GL020974
- Nakamura H, Ichikawa H, Nishina A (2007) Numerical study of the dynamics of the Ryukyu Current system. *J Geophys Res: Oceans* 112:C04016. doi:10.1029/2006JC003595

- Petersen MR, Williams SJ, Maltrud ME, Hecht MW, Hamann B (2013) A three-dimensional eddy census of a high-resolution global ocean simulation. *J Geophys Res: Oceans* 118(4):1759–1774. doi:[10.1002/jgrc.20155](https://doi.org/10.1002/jgrc.20155)
- Qiu B (1999) Seasonal eddy field modulation of the North Pacific Subtropical Countercurrent: TOPEX/Poseidon observations and theory. *J Phys Oceanogr* 29(10):2471–2486. doi:[10.1175/1520-0485\(1999\)029<2471:SEFMOT>2.0.CO;2](https://doi.org/10.1175/1520-0485(1999)029<2471:SEFMOT>2.0.CO;2)
- Qiu B (2001) Kuroshio and Oyashio currents. In: Thorpe SA (ed) *A derivative of the Encyclopedia of Ocean Sciences: ocean currents*. Academic, Waltham, pp 1413–1425
- Qiu B, Chen S (2013) Concurrent decadal mesoscale eddy modulations in the western North Pacific subtropical gyre. *J Phys Oceanogr* 43(2):344–358. doi:[10.1175/JPO-D-12-0133.1](https://doi.org/10.1175/JPO-D-12-0133.1)
- Rio MH, Guinehut S, Larnicol G (2011) New CNES-CLS09 global mean dynamic topography computed from the combination of GRACE data, altimetry, and in situ measurements. *J Geophys Res Oceans* 116:C07018. doi:[10.1029/2010JC006505](https://doi.org/10.1029/2010JC006505)
- Sheu W-J, Wu C-R, Oey L-Y (2010) Blocking and westward passage of eddies in the Luzon Strait. *Deep Sea Res Part II* 57(19):1783–1791. doi:[10.1016/j.dsr2.2010.04.004](https://doi.org/10.1016/j.dsr2.2010.04.004)
- Smith DC, O'Brien J (1983) The interaction of a two-layer isolated mesoscale eddy with bottom topography. *J Phys Oceanogr* 13(9):1681–1697. doi:[10.1175/1520-0485\(1983\)013<1681:TIOATL>2.0.CO;2](https://doi.org/10.1175/1520-0485(1983)013<1681:TIOATL>2.0.CO;2)
- Souza JMAC, de Boyer Montégut C, Le Traon PY (2011) Comparison between three implementations of automatic identification algorithms for the quantification and characterization of mesoscale eddies in the South Atlantic Ocean. *Ocean Sci* 7(3):317–334. doi:[10.5194/os-7-317-2011](https://doi.org/10.5194/os-7-317-2011)
- Thoppil PG, Metzger EJ, Hurlburt HE, Smedstad OM, Ichikawa H (2016) The current system east of the Ryukyu Islands as revealed by a global ocean reanalysis. *Prog Oceanogr* 141:239–258. doi:[10.1016/j.pocean.2015.12.013](https://doi.org/10.1016/j.pocean.2015.12.013)
- Tsai CJ, Andres M, Jan S, Mensah V, Sanford TB, Lien RC, Lee CM (2015) Eddy–Kuroshio interaction processes revealed by mooring observations off Taiwan and Luzon. *Geophys Res Lett* 42:8098–8105. doi:[10.1002/2015GL065814](https://doi.org/10.1002/2015GL065814)
- Waterman S, Hogg NG, Jayne SR (2011) Eddy–mean flow interaction in the Kuroshio Extension region. *J Phys Oceanogr* 41(6):1182–1208. doi:[10.1175/2010JPO4564.1](https://doi.org/10.1175/2010JPO4564.1)
- Yang Y, Liu C-T, Hu J-H, Koga M (1999) Taiwan current (Kuroshio) and impinging eddies. *J Oceanogr* 55(5):609–617. doi:[10.1007/892819134](https://doi.org/10.1007/892819134)
- Yang G, Wang F, Li Y, Lin P (2013) Mesoscale eddies in the northwestern subtropical Pacific Ocean: statistical characteristics and three-dimensional structures. *J Geophys Res: Oceans* 118(4):1906–1925. doi:[10.1002/jgrc.20164](https://doi.org/10.1002/jgrc.20164)
- Zhai X, Johnson HL, Marshall DP (2010) Significant sink of ocean-eddy energy near western boundaries. *Nature Geosci* 3(9):608–612. doi:[10.1038/ngeo943](https://doi.org/10.1038/ngeo943)
- Zhang D, Lee TN, Johns WE, Liu C-T, Zantopp R (2001) The Kuroshio east of Taiwan: modes of variability and relationship to interior ocean mesoscale eddies. *J Phys Oceanogr* 31(4):1054–1074. doi:[10.1175/1520-0485\(2001\)031<1054:TKEOTM>2.0.CO;2](https://doi.org/10.1175/1520-0485(2001)031<1054:TKEOTM>2.0.CO;2)
- Zheng Q, Tai C-K, Hu J, Lin H, Zhang R-H, Su F-C, Yang X (2011) Satellite altimeter observations of nonlinear Rossby eddy–Kuroshio interaction at the Luzon Strait. *J Oceanogr* 67(4):365–376. doi:[10.1007/s10872-011-0035-2](https://doi.org/10.1007/s10872-011-0035-2)
- Zhu X-H, Ichikawa H, Ichikawa K, Takeuchi K (2004) Volume transport variability southeast of Okinawa Island estimated from satellite altimeter data. *J Oceanogr* 60(6):953–962. doi:[10.1007/s10872-005-0004-8](https://doi.org/10.1007/s10872-005-0004-8)